a radiative model that incorporates scattering in the infrared. (CO_2 ice, unlike water or water ice, is a nearly pure scatterer at most infrared wavelengths[18].) The radiative effect of CO_2 clouds can, however, be estimated qualitatively: because CO_2 clouds are poor absorbers, their contribution to the greenhouse effect should be relatively small, so their primary influence should be to cool the Earth by increasing its albedo.

The points where CO_2 clouds begin to form in our model are indicated by the solid curves in Fig. 2. We have divided the earlier phase of the Earth's history into two parts, labelled 'case 2' and 'case 3'. When S_{eff} is less than ~0.92 (earlier than ~1 Gyr ago[3]) our model predicts that CO_2 clouds would start to form at the poles (case 2). When S_{eff} is less than ~0.8 (earlier than ~3 Gyr ago[3]) CO_2 cloud cover would extend all the way down to the Equator. It is uncertain what the albedo of such a CO_2 cloud-covered planet would be. If it were as high as 0.8, our model predicts that the Earth would not be able to emerge from that state, even at the present solar luminosity. Thus, if the Earth had experienced runaway glaciation before ~3 Gyr ago, the situation might have been effectively irreversible.

How the early Earth managed to avoid becoming globally glaciated is a question of considerable importance to those interested in the general problem of planetary habitability. One possibility is that the Earth remained in a low-ice state simply because it started out hot following accretion: a dense, CO_2-N_2-H_2O atmosphere that was initially warm would be free of CO_2 clouds even at 70% of present solar luminosity (Fig. 3). Alternatively, the presence of additional greenhouse gases, such as NH_3 (ref. 4) or CH_4 (ref. 19), might have kept the atmosphere warm enough to prevent CO_2 from condensing. In either case, the explanation for why Earth's climate has remained stable is more complex than has been previously assumed. □

Received 24 April; accepted 28 July 1992.

1. Budyko, M. I. *Tellus* **21,** 611–619 (1969).
2. Sellers, W. D. *J. appl. Met.* **8,** 392–400 (1969).
3. Gough, D. O. *Solar Phys.* **74,** 21–34 (1981).
4. Sagan, C. & Mullen, G. *Science* **177,** 52–56 (1972).
5. Owen, T., Cess, R. D. & Ramanathan, V. *Nature* **277,** 640–642 (1979).
6. Walker, J. C. G., Hays, P. B. & Kasting, J. F. *J. geophys. Res.* **86,** 9776–9782 (1981).
7. Marshall, H. G., Walker, J. C. G. & Kuhn, W. R. *J. geophys. Res.* **93,** 791–801 (1988).
8. Kasting, J. F. *Icarus* **94,** 1–13 (1991).
9. Allart, J. H., in *The Early History of the Earth* (ed. Windley, B. F.) 177–189 (Wiley, New York, 1976).
10. Worsley, T. R. & Kidder, D. L. *Geology* **19,** 1161–1164 (1992).
11. Walter, M. *Am. Scient.* **67,** 142 (1979).
12. McWilliams, M. O. & McElhinney, M. W. *J. Geol.* **88,** 1–26 (1980).
13. Hambrey, M. J. & Harland, W. B. *Palaeogeogr. Palaeoclimatol. Palaeoecol.* **51,** 255–272 (1985).
14. Sundquist, E. T. *Quat. Sci. Rev.* **10,** 283–296 (1991).
15. Cahalan, R. F. & North, G. R. *J. atmos. Sci.* **36,** 1178–1188 (1979).
16. Holland, H. D. *The Chemistry of the Atmosphere and Oceans* (Wiley, New York, 1978).
17. Kasting, J. F., Whitmire, D. P. & Reynolds, R. T. *Icarus* (in the press).
18. Warren, S. G. *Appl. Opt.* **25,** 2650–2674 (1986).
19. Kiehl, J. T. & Dickenson, R. E. *J. geophys. Res.* **92,** 2991–2998 (1986).
20. Kasting, J. F. & Ackerman, T. P. *Science* **234,** 1383–1385 (1986).
21. North, G. R., Cahalan, R. F. & Coakley, J. A. *Rev. Geophys.* **19,** 91–121 (1981).
22. North, G. R. & Coakley, J. A. *J. atmos. Sci.* **36,** 1189–1204 (1979).
23. Rossow, W. B., Henderson-Sellers, A. & Weinrich, S. K. *Science* **217,** 1245–1247 (1982).

ACKNOWLEDGEMENTS. We thank A. Lapenis for discussions and C. Sagan for a review. K.C. was supported by the NSF under a grant awarded in 1991.

Role of pore fluids in the generation of seismic precursors to shear fracture

P. R. Sammonds*, P. G. Meredith* & I. G. Main†

* Department of Geological Sciences, University College London, Gower Street, London WC1E 6BT, UK
† Department of Geology & Geophysics, University of Edinburgh, Grant Institute, West Mains Road, Edinburgh EH9 3JW, UK

A SYSTEMATIC study of temporal changes in seismic *b*-values (defined as the log-linear slope of the earthquake frequency–magnitude distribution) has shown that large earthquakes are often preceded by an intermediate-term increase in *b*, followed by a decrease in the months to weeks before the earthquake[1]. The onset of the *b*-value increase can precede earthquake occurrence by as much as 7 years. A recently proposed fracture mechanics model of the earthquake source[2] explains these temporal fluctuations in *b* in terms of the underlying physical processes of time-varying applied stress and crack growth. The model predicts two minima in *b*, separated by a short-lived maximum. Here we report the results of controlled laboratory deformation experiments, done in simulated upper-crustal conditions on both air-dried and water-saturated rock specimens. As found in previous experiments[3–5], shear fracture in dry specimens is characterized by a decline in *b* during anelastic deformation to a single minimum reached just before failure. But in water-saturated specimens, when pore-fluid volume is kept constant by servo-control we also observe a second, intermediate-term *b*-value minimum, so reproducing the double *b*-value anomaly predicted by the model[2].

The fracture mechanics model of Main *et al.*[2] is summarized in Fig. 1. In nature, because crustal deformation is accompanied and accomplished by microcracking and small earthquakes[6], sometimes coupled with aseismic deformation, the crust will respond to remotely applied tectonic loading by deforming anelastically; it shows both strain-hardening and strain-softening phases, and a dynamic failure stress lower than peak stress (Fig. 1*a*). Laboratory experiments have shown that a principal flaw under the action of remotely applied stress and stress corrosion processes will extend in a strongly nonlinear fashion[7] (Fig. 1*b*) from an initial length x_0 at time t_0 to effectively infinite length at time t_f. Combining the effects of stress and

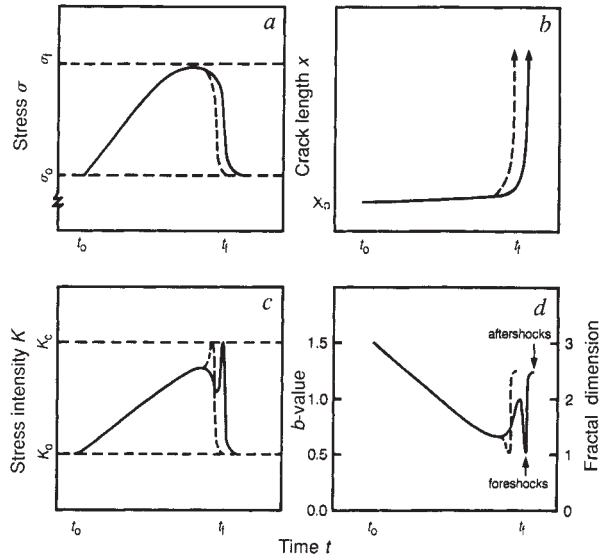

FIG. 1 Fracture mechanics model of the *b*-value anomaly for anelastic failure (precursory strain energy release model)[2]. *a*, Stress–time behaviour for rock deformation; *b*, acceleration of crack tip to critical failure; *c*, combined effects of the stress and crack length of the stress intensity factor, *K*. *d*, Because *b* is negatively correlated and linearly related to *K*, the model predicts both an intermediate-term and a short-term *b*-value minimum. A single minimum will be produced where failure occurs during an earlier part of the cycle (dashed line). σ_0, Initial stress at time t_0; σ_f, nominal failure stress (peak stress); t_0, onset time of loading; t_f, dynamic failure time; x_0, crack length at time t_0; K_c, critical stress intensity (fracture toughness); K_0, stress intensity at time t_0.

crack growth behaviour, the stress intensity factor K (defined by $K = Y\sigma x^{1/2}$, where σ is the remotely applied stress and Y is a geometric factor) is modelled as increasing gradually from a value K_0 at time t_0 to a level approaching a critical value for macroscopic failure K_c (Fig. 1*c*). But decreasing stress in the strain-softening phase reduces K temporarily before the effect of the accelerating crack length begins to dominate, resulting in a rapid increase in K to critical failure. As it has been found experimentally that the stress intensity factor of the principal flaw is negatively correlated to the *b*-value derived from monitoring acoustic emissions produced by microcracking as the flaw advances[8], the model predicts both an intermediate-term and short-term *b*-value anomaly in the form of a double minimum, associated with K reaching a maximum first at peak stress and then at the onset of dynamic failure (Fig. 1*d*). A single minimum in *b* will, however, be produced where failure occurs during an

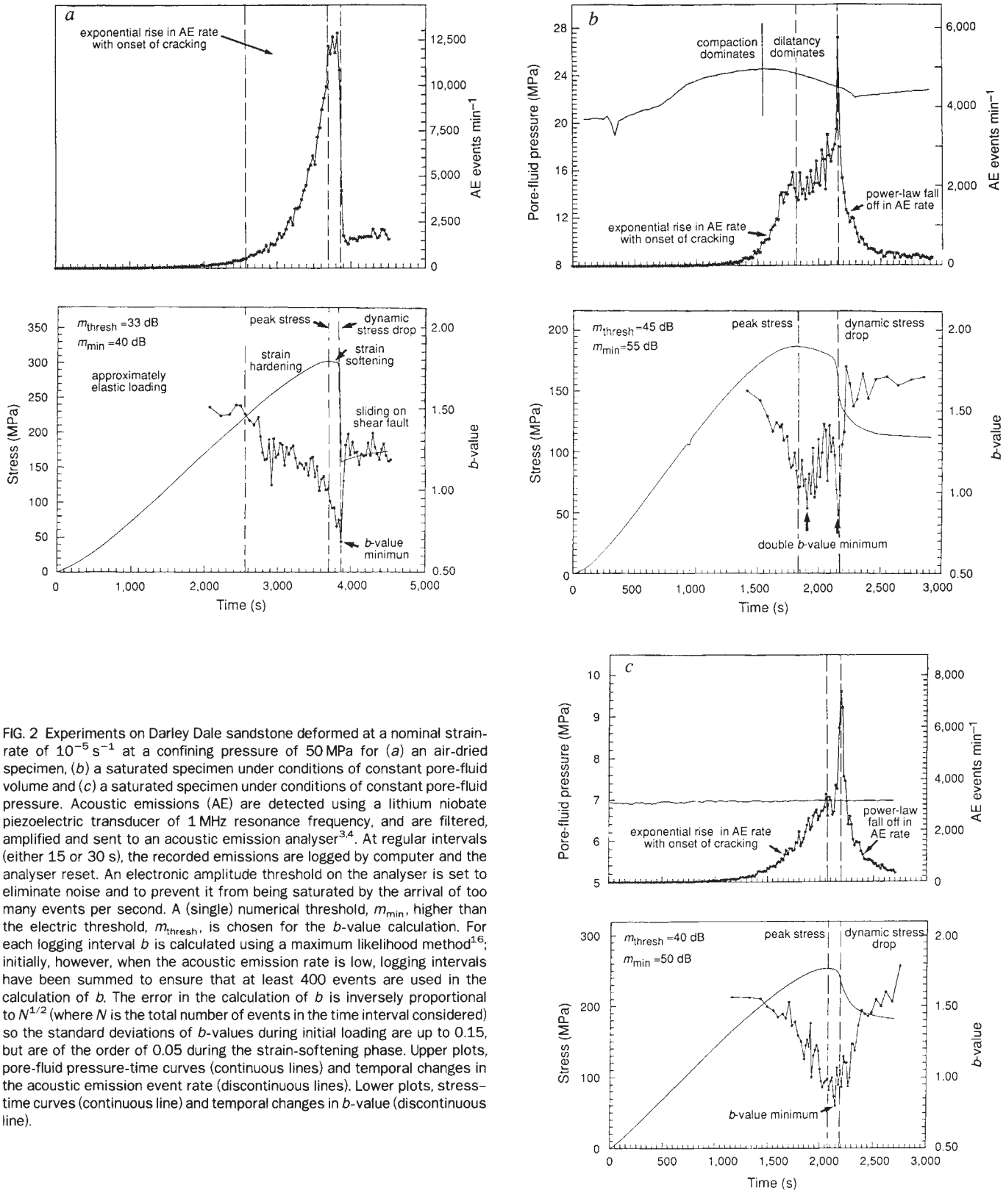

FIG. 2 Experiments on Darley Dale sandstone deformed at a nominal strain-rate of 10^{-5} s^{-1} at a confining pressure of 50 MPa for (*a*) an air-dried specimen, (*b*) a saturated specimen under conditions of constant pore-fluid volume and (*c*) a saturated specimen under conditions of constant pore-fluid pressure. Acoustic emissions (AE) are detected using a lithium niobate piezoelectric transducer of 1 MHz resonance frequency, and are filtered, amplified and sent to an acoustic emission analyser[3,4]. At regular intervals (either 15 or 30 s), the recorded emissions are logged by computer and the analyser reset. An electronic amplitude threshold on the analyser is set to eliminate noise and to prevent it from being saturated by the arrival of too many events per second. A (single) numerical threshold, m_{min}, higher than the electric threshold, m_{thresh}, is chosen for the *b*-value calculation. For each logging interval *b* is calculated using a maximum likelihood method[16]; initially, however, when the acoustic emission rate is low, logging intervals have been summed to ensure that at least 400 events are used in the calculation of *b*. The error in the calculation of *b* is inversely proportional to $N^{1/2}$ (where N is the total number of events in the time interval considered) so the standard deviations of *b*-values during initial loading are up to 0.15, but are of the order of 0.05 during the strain-softening phase. Upper plots, pore-fluid pressure-time curves (continuous lines) and temporal changes in the acoustic emission event rate (discontinuous lines). Lower plots, stress–time curves (continuous line) and temporal changes in *b*-value (discontinuous line).

earlier part of the cycle (dashed lines in Fig. 1). Calculations of t_f for conditions found on the San Andreas fault suggest rupture times of 150 to 220 years, but with sudden crack length changes which give rise to seismic precursors occurring only in the final 10 years[9].

To test this model we have done triaxial deformation experiments on initially intact specimens of Darley Dale sandstone, a well-indurated felspathic sandstone with a siliceous cementing material, selected because it shows distinct phases of both strain hardening and strain softening during deformation. Right cylindrical specimens 15 mm in diameter by 45 mm in length, jacketed in a ductile copper sleeve, were deformed in compression in a high-pressure triaxial cell, incorporating a servo-controlled pore-fluid pressure intensifier and volume monitor. An all-round hydrostatic pressure is first applied to the specimen and maintained at a set value (the 'confining pressure'). The pore-fluid intensifier piston is advanced to force high-pressure water into the specimen and left to equilibrate. Then an axial load is applied to the rock specimen by a 200-kN servo-controlled actuator at constant displacement rate. During deformation of the specimen the pore-fluid intensifier can be set to maintain either a constant pore-fluid pressure or constant pore-fluid volume. Acoustic emission is detected continuously using a transducer located close to the specimen in the hollow lower loading piston inside the pressure vessel.

Figure 2*a* shows acoustic emission results from an experiment on an air-dried sandstone specimen. Initial compaction of the specimen is associated with low acoustic emission. At ~50% of peak stress, microcrack initiation and extension commences and the rate of acoustic emission activity increases exponentially. Peak stress is followed by a small but significant period of strain softening leading to dynamic failure. Failure occurs on a well-defined fault plane oriented at between 30° and 35° to the maximum principal compression axis. During the quasi-linear elastic phase of loading, the *b*-value is high, fluctuating around an average of ~1.5. As deformation proceeds, *b* decreases steadily; then just before dynamic failure, it dips sharply towards ~0.5. It then recovers to ~1.2 during the period of frictional sliding that follows failure. These experimentally measured *b*-values roughly agree with those measured in nature, with background seismicity often associated with $b \geq 1$ and earthquake foreshocks with $b = 0.5$ (ref. 10), and with experimental results presented previously[3-5]. Observations of the intermediate-term increase in *b* followed by a decrease were not, however, reproduced.

By contrast, Fig. 2*b* shows results from an experiment where the specimen was deformed in the presence of water as a pore fluid held at constant pore-fluid volume. (These conditions roughly correspond to a depth of 2–3 km with a pore-fluid pressure that is initially hydrostatic.) On comparison with Fig. 2*a*, the stress–time curve shows that the specimen is considerably weaker because of the combined chemical and mechanical influences of the pressurized pore fluid, and that dynamic failure is now preceded by a prolonged period of strain softening due to dilatancy hardening caused by a decreasing pore-fluid pressure. After a period of stability during initial loading, the pore-fluid pressure starts to increase as the specimen is compacted, peaking as the opening of new dilational microcracks begins to dominate over the closure of pre-existing cracks and flaws, and then falls, finally reaching an essentially constant level during the frictional sliding phase. The acoustic emission rate increases roughly exponentially with time, reaching an inflection point around peak stress. After failure the rate decreases roughly according to a power law, consistent with observations of aftershock sequences[11]. But it is the *b*-value that show the most interesting behaviour. The experiment again reproduces the now-familiar short-term *b*-value minimum, but we now observe an intermediate-term *b*-value minimum, followed by a recovery before dipping to the second minimum just before the dynamic stress drop. Of all the conditions under which we have deformed rocks, this test condition of shear fracture at controlled constant pore-fluid volume is the only one to show the distinctive 'double minimum' in *b*. The recovery in *b* and short-term drop correspond to the type of anomaly reported by Smith[1].

Finally, in Fig. 2*c* we present results from an experiment done under conditions of constant pore-fluid pressure. The application of even a small constant pore-fluid pressure to the specimen results in a stress–time curve that shows only a short strain-softening phase and small dynamic stress drop. A single *b*-value minimum is observed just before the dynamic failure under these conditions.

Our experimental results reveal an exponentially increasing rate of acoustic emission during loading under all three conditions up to peak stress, but for the experiment at constant pore-fluid volume there is abrupt flattening of the rate. This last case we interpret as being caused by local dilatancy hardening resulting from falling pore-water pressure, although the specimen is softening overall. This has the effect of extending the post-peak stress deformation before dynamic failure occurs. A declining *b*-value is observed initially for anelastic deformation for all three test conditions. For the experiments with air-dry specimens or constant pore-fluid pressure, the decrease in *b* leads directly to dynamic failure immediately following minimum *b*. Even though overall stress was falling as the specimen strain-softened, this was not sufficient to relieve the stress intensity driving these systems to failure. For the experiment at constant pore-fluid volume, the *b*-value first recovered before falling to a second minimum at failure. In this last case, the combined effects of falling applied stress and falling pore-fluid pressure allowed a relaxation in stress intensity, with damage accumulation still progressing but with the formation of the shear fault delayed.

The earthquake source model of Main *et al.*[2] requires a prolonged strain-softening phase before dynamic failure if a double *b*-value minimum is to be observed in nature. This could be promoted by a falling pore-fluid pressure at constant pore-fluid volume. (The model also accounts for *b*-value behaviour for a short strain-softening phase). Nonhydrostatic pore fluid pressures in the crust require that rock permeability is low or that low-permeability rock encloses rock of higher permability. There is considerable geological and geophysical evidence for this[12,13], and time-dependent changes in permeability in the crust have been roughly quantified[12]. The departure of pore-fluid pressure from hydrostatic has also been cited as an important mechanism in the 'dilatancy-diffusion' model of the earthquake source[14] and to account for the 'weakness' of the San Andreas fault[15]. Extrapolation of recent calculations[12] suggest that small changes in pore-fluid pressure needed to prolong the strain softening phase could occur within 10 years, but a full quantitative description of the model of Main *et al.*[2] awaits an understanding of crack development, porosity and permeability changes for the complete deformation cycle. □

Received 4 March; accepted 3 August 1992.

1. Smith, W. D. *Nature* **289,** 136–139 (1981).
2. Main, I. G., Meredith, P. G. & Jones, C. *Geophys. J.* **96,** 131–138 (1989).
3. Meredith, P. G., Main, I. G. & Jones, C. *Tectonophysics* **175,** 249–268 (1990).
4. Sammonds, P. R., Ayling, M. R., Meredith, P. G., Murrell, S. A. F. & Jones, C. in *Rock at Great Depth* (eds Maury, V. & Fourmaintraux, D.) (Balkema, Rotterdam, 1989).
5. Lockner, D. A., Byerlee, J. D., Kiksenko, V., Ponomarev, A. & Sidorin, A. *Nature* **350,** 39–42 (1991).
6. Mogi, K. *Earthquake Prediction* (Academic, London, 1985).
7. Atkinson, B. K. & Meredith, P. G. in *Fracture Mechanics of Rock* (ed. Atkinson, B. K.) (Academic, London, 1987).
8. Meredith, P. G. & Atkinson, B. K. *Geophys. J.R. astr. Soc.* **75,** 1–21 (1983).
9. Main, I. *Geophys. J.* **92,** 455–464 (1988).
10. von Seggern, D. *Geophys. J.R. astr. Soc.* **86,** 815–838 (1980).
11. Utsu, T. *Geophys. Mag.* **30,** 521–605 (1961).
12. Nur, A. M. & Walder, J. in *The Role of Fluids in Crustal Processes* (panel co-chair Bredehoeft, J. D. & Norton, D. L.) (National Academy Press, Washington DC, 1990).
13. Marquis, G. & Hyndman, R. D. *Geophys. J. int.* **110,** 91–105 (1992).
14. Scholz, C. H., Sykes, L. R. & Aggarwal, Y. P. *Science* **181,** 803–810 (1973).
15. Rice, J. R. *Extended Abstr. int. Symp. Earthq. Source Phys. Earthq. Precursors* 7–11 (Univ. of Tokyo, 1990).
16. Aki, K. *Bull. Earthq. Res. Inst. Tokyo Univ.* **43,** 237–239 (1965).

ACKNOWLEDGEMENTS. Financial support for this work was provided by the U.K. NERC.